Three dimensional toughening mechanism in Haversian cortical bone modulating mechanical stimuli to osteocytes

Elisa Budyn, Gaëlle Belot, Thierry Hoc, Morad Bensidhoum, Hervé Petite

CSMA 2013
11e Colloque National en Calcul des Structures
13-17 Mai 2013

Three dimensional toughening mechanism in Haversian cortical bone modulating mechanical stimuli to osteocytes

Elisa BUDYN[1], Gaëlle BELOT[2], Thierry HOC[3], Morad BENSIDHOUM[4], Hervé PETITE[5]

[1] University of Illinois at Chicago, Department of Mechanical and Bio Engineering, ebudyn@uic.edu
[2] University of Illinois at Chicago, Department of Mechanical Engineering, gbelot2@uic.edu
[3] Ecole Centrale Lyon, LTDS, thierry.hoc@ec-lyon.fr
[4] Université Paris 7, B2OA, morad.bensidhoum@paris7.jussieu.fr
[5] Université Paris Diderot, B2OA, herve.petite@univ-paris-diderot.fr

Résumé — Haversian cortical bone is a mineralised tissue maintained by trapped ostecytes that detect mechanical stimuli produced by naturally occurring micro cracks. We present a method to evaluated Haversian cortical bone toughness from the total energy variation of bone mechanical response during three point bending tests. The three characteristic directions of Haversian bone are tested : longitudinal, anti-plane longitudinal and transverse.
Mots clés — cortical bone, toughness, energy variation

1 Introduction

Haversian cortical bone is a mineralised tissue with a composite microstructure [1, 2] that undergoes under daily loading different types of damage that is either localised such as micro cracks over few micron length that are easily seen under light microscopy [3, 4] or is more diffuse and difficult to image and characterise [5]. At the micro scale or osteonal scale, Haversian cortical bone displays densely packed cylinder-shaped structures called osteons formed of concentric lamellae of few micron thickness embedded in an interstitial matrix composed of former osteon remnants. Osteons are surrounded by nearly $5\mu m$ thick lamella interfaces [6, 7] called cement lines. Through the osteons run Haversian canals that contain blood capillaries and nerves. As a living tissue, bone heterogeneous microstructure is formed by a continuous self-healing process called remodeling that repairs and adapts the tissue microstructure to external mechanical load [8]. At the sub-micro level, cortical bone is composed of an organic phase made of fibrils that mainly contain collagen Type I and hydroxyapatite minerals [9]. Due to its high mineral content [10], bone is mostly elastic and brittle, which leads to the development of micro damage and microcracks [11, 12, 13] under daily exercise.

Bone cells called osteocytes maintained the living tissue and are located throughout the mineralised microstructure. Osteocytes are mechano-sensitive and detect mechanical stimulation in their micro environment, to which they respond by adapting their internal biology. However in situ mechanical cell micro environment is difficult to precisely quantify. To measure the stress field seen by osteocytes and visualise the diffuse damage near micro cracks, we present a method that couples reflective light microscopy imaging, chemical staining [14], digital image correlation of the local displacement field and an energy analysis of the sample macroscopic response. The method is applied to micro tension tests of millimetric samples collected in the three characteristic orientations of fresh human Haversian cortical bone.

2 Material and method

In the experimental setting, human cortical bone millimetric samples of dimensions given in Table 1 are subjected to a three point bending tests applied by a miniaturised device that fits under a light microscope [16] shown in Figure 1. The cadaveric specimens are harvested from the fresh posterior femoral mid-diaphyses of elderly woman over 70. The sample global force and displacement are measured by two sensors. Concomitantly the bone microstructure surface is locally observed in the anti-plane lon-

gitudinal direction of the osteons after fine polishing [16] as shown in Figure 1(b). As the device advance is 0 2μms^{-1}, the mechanical test is considered quasi-static. At consecutive load steps, grey scale $2048 \times 2048\, px^2$ images are acquired at characteristic crack growths by a camera with an optical resolution of 1 50 1 55 1 57$\mu m\, px^{-1}$ [16]. At each step, the discrete displacements of discrete points on a $n_x \times n_y$ grid in Figure 1(b) are calculated by digital image cross-correlation (DIC) [15, 16]. This grid defines a $W_2 \times H_2$ window of interest where the failure occurs shown in Figure 1. The samples are initially pre cracked and display initial crack indent a_0.

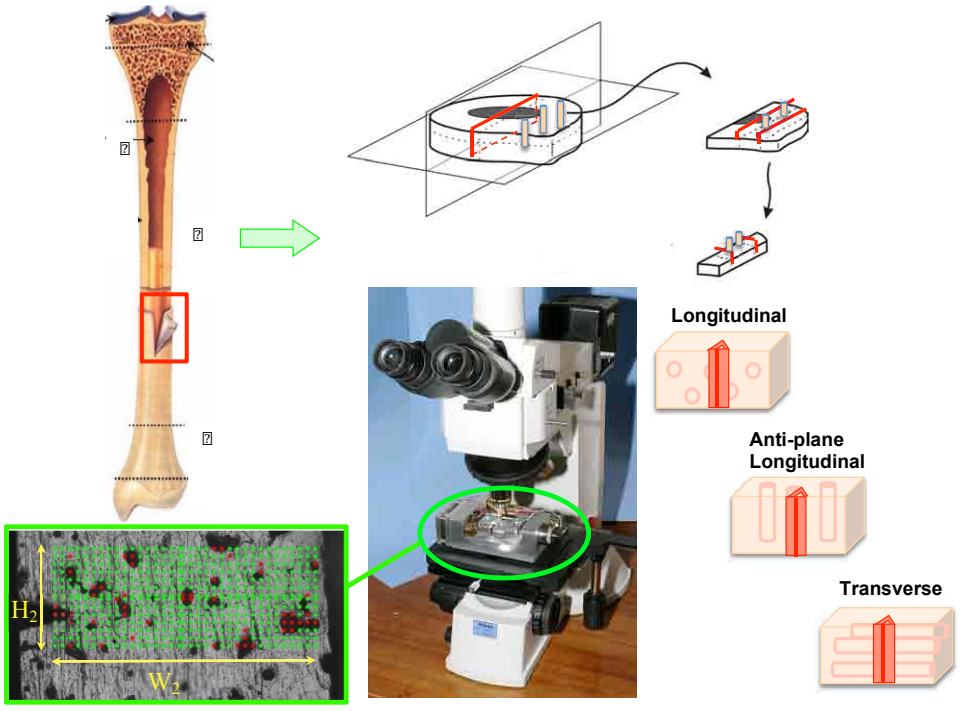

Fig. 1 – Micro three point bending experimental setting and sample preparation.

Tableau 1 – Bone sample dimensions (note the Height H represents the distance between the two pods of the three point bending device).

Tests	width W	thickness t	height H	W_2	H_2	a_0	n_x	n_y
	mm	mm	mm	μm	μm	μm		
L	2.03	1.77	4	1441	528	608	31	12
AL	1.97	1.87	4	1664	621	348	35	14
T	2.09	1.72	4	1607	728	350	33	16

3 Results

The local displacements calculated by Digital Image cross-Correlation show the crack discontinuities in Figure 3 for the three point bending tests in the three characteristic orientations of bone.

The global load-displacement curves of the thee point bending tests are shown in Figure 4.

3.1 Stress-intensity factor calculations using a semi-analytical method

During a three point bending test, mode I opening is dominant and the stress intensity factors in mode I at the major crack tip shown in Figure 5 can be estimated by a semi-analytical formulation [20, 21] as follows :

$$K_I = \frac{P}{t\sqrt{W}}\, f(\frac{a}{W}) \tag{1}$$

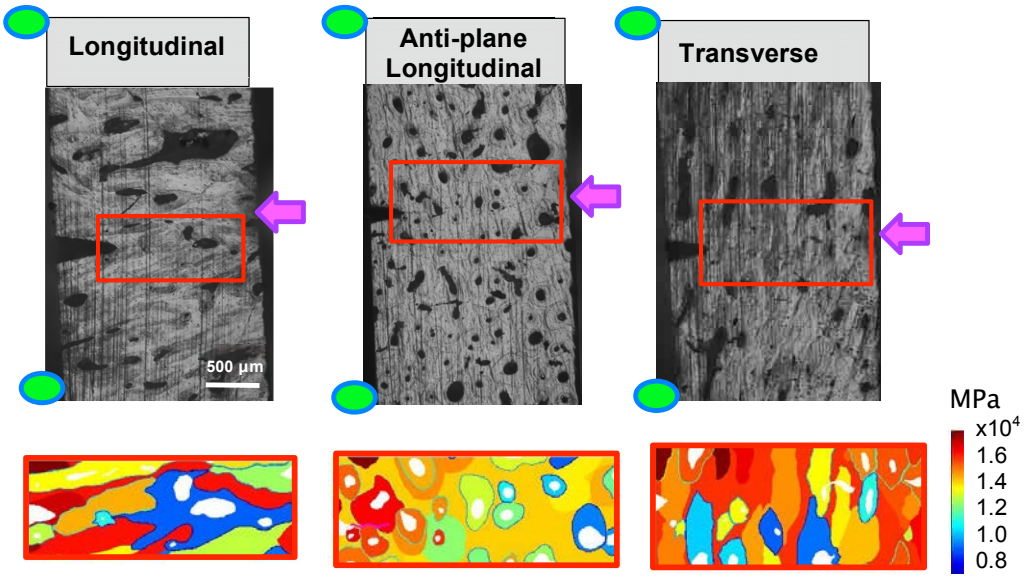

Fig. 2 – Young's moduli map in the windows of observation in the vicinity of the crack indent of the 3 bone samples where the osteons are either in the longitudinal, anti-plane longitudinal or transverse directions respectively.

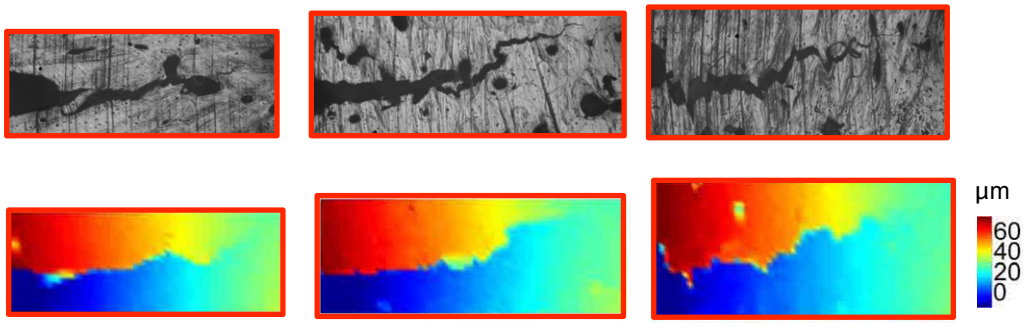

Fig. 3 – Vertical displacement field calculated by Digital Image cross-Correlation as the main cracks grow in the 3 bone samples where the osteons are either in the longitudinal, anti-plane longitudinal or transverse directions respectively.

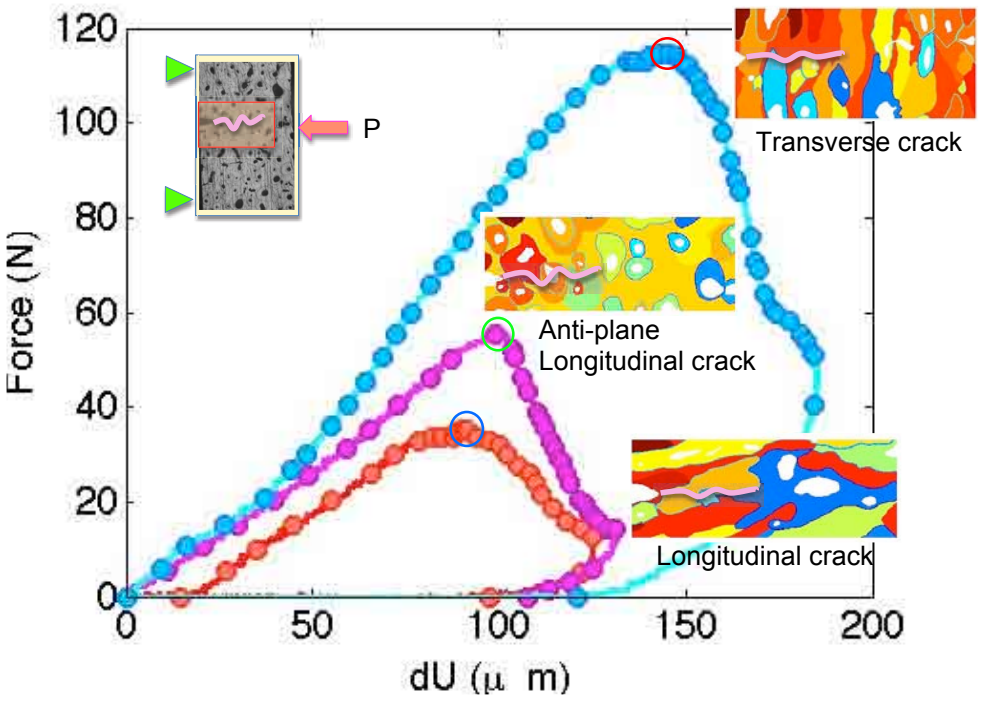

Fig. 4 – Load deflection curves of three aversion cortical bone samples cut in the three bone characteristic directions : longitudinal, anti-plane longitudinal, transverse.

where $f(\frac{a}{W})$ is defined as follows :

$$f(\frac{a}{W}) = \frac{3\frac{H}{W}\sqrt{\frac{a}{W}}}{2(1+2\frac{a}{W})(1-\frac{a}{W})^{3\ 2}}[1\ 99 - \frac{a}{W}(1-\frac{a}{W})(2\ 15 - 3\ 13\frac{a}{W} + 2\ 7(\frac{a}{W})^2)] \quad (2)$$

where W is the specimen width and t its thickness, a is the equivalent crack length and H is the support span of the three point bending test device. However note that Equations (1) and (2) are valid for a three point bending test of a homogeneous material, which is an approximation here. Following the ASTM Standard E399 [22], a semi-analytical critical stress intensity factor for each tests can be calculated as the stress intensity factor value corresponding to the maximum load. The values are given in Table 2.

Tableau 2 – Critical mode I stress-intensity factors calculated by ASTM Standard E399 method [22].

Bone	Orientation	Geometry	$P_{max}(N)$	K_{Ic} (MPa.m$^{1\ 2}$)
Human femur	Anti-plane longitudinal	SEN(B)	55.4	4.32
Human femur	In-plane longitudinal	SEN(B)	35.2	2.74
Human femur	Transverse	SEN(B)	114.4	9.87

3.2 Stress-intensity factor calculations using the variation of the total energy

At each loading step, the sample can be imaged and the micro crack growth and arrest are determined. The balance between the internal strain energy of the mineralised tissue fracturing in quasi-static condition and the external energy makes it possible to measure the work of separation along the crack edges at the micro scale and the evolution of the stress intensity factors (SIFs) at the advancing crack tips [17, 18, 19]. The evolution of the stress intensity factors is tracked in the three characteristic directions of bone : longitudinal, anti-plane longitudinal and transverse. In a first approach, the bone samples of elderly women are assumed linear-elastic materials undergoing brittle fracture with no cohesive zone where the plastic energy and the cohesive energy are not calculated. Under this assumption, all the energy

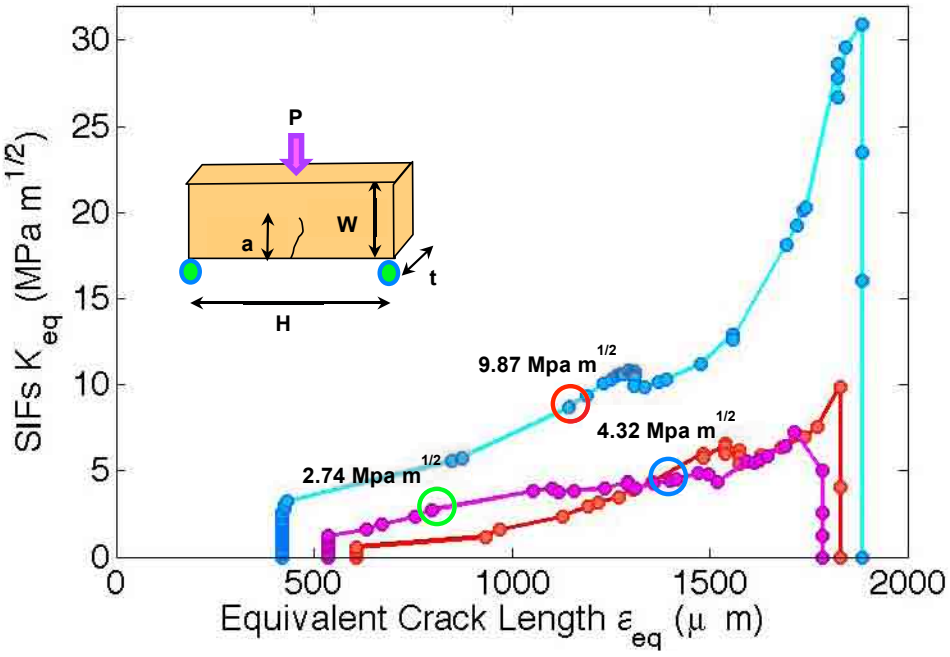

Fig. 5 – The stress intensity factors are calculated following ASTM Standard E399 which uses a analytical formula for homogeneous materials.

in the system is dissipated during the crack advance to separate the surfaces of the cracks. The energy release rate during each crack advance can then be calculated from the the total energy variation in Figure 4 by :

$$G = -\frac{\partial \mathcal{W}}{\partial S} \tag{3}$$

where $\mathcal{W}$ is the total energy of the system and S is the crack surface.

The total energy $\mathcal{W}$ accumulated in the material is expressed by :

$$\mathcal{W} = \mathcal{W}_{int} - \mathcal{W}_{ext} \tag{4}$$

where $\mathcal{W}_{int}$ is the strain energy stored in the body and $\mathcal{W}_{ext}$ the work done by external force. The strain energy $\mathcal{W}_{int}$ can be defined as follows :

$$\mathcal{W}_{int} = \frac{1}{2} P \cdot u \tag{5}$$

and the work done by external force $\mathcal{W}_{ext}$ by :

$$\mathcal{W}_{ext} = P \cdot u \tag{6}$$

where P and u are the measured load and the applied displacement on the sample during the three point bending test. By substituting Equations (5) and (6) into Equation (4), the total energy $\mathcal{W}$ in the sample becomes :

$$\mathcal{W} = -\frac{1}{2} P \cdot u \tag{7}$$

The energy release rate G measures the energy released during the extension of a crack and is defined by :

$$G = -\frac{\partial \mathcal{W}}{\partial S} \tag{8}$$

where dS is the crack surface equal to $S = a \cdot t$ where a is the real crack length and t the sample thickness. Using a forward Euler linearisation, the energy release rate at step $n+1$ can be approximated by :

$$G^{n+1} = -\frac{\mathcal{W}^{n+1} - \mathcal{W}^{n}}{S^{n+1} - S^{n}} = -\frac{1}{t}\frac{\mathcal{W}^{n+1} - \mathcal{W}^{n}}{a^{n+1} - a^{n}} \tag{9}$$

The equivalent stress-intensity factor K_{eq} in 2D can be defined by :

$$K_{eq} = \sqrt{K_I^2 + K_{II}^2} \tag{10}$$

where K_I and K_{II} are the values of the stress-intensity factor respectively in mode I and mode II. For linear-elastic materials, K_{eq} can be expressed by [18, 19] :

$$G = \frac{K_{eq}^2}{E^\star} \tag{11}$$

where $E^\star$ is the appropriate elastic modulus ($E^\star = E$ in plane stress and $E^\star = E/(1 \quad ^2)$ in plane strain. E is Young's modulus and is Poisson's ratio) and μ is the shear modulus [18, 19]. Because we are observing the surface of the sample, whose thickness is assumed small, we apply a plane-stress approximation. By substituting Equation (7) into Equation (9), the latter into Equation (11), the equivalent stress-intensity factor K_{eq} at step $n+1$ can be rewritten as follows :

$$K_{eq}^{n+1} = \sqrt{\frac{E}{2t} \cdot \frac{P^{n+1}.u^{n+1} \quad P^n.u^n}{a^{n+1} \quad a^n}} \tag{12}$$

In the case of multiple cracks growing within the same step, we can write :

$$\frac{\mathcal{W}}{a} = \frac{\mathcal{W}}{a} = \frac{{}_j \ \mathcal{W}_j}{{}_i \ a_i} = {}_j \left(\frac{\mathcal{W}_j}{{}_i \ a_i} \right) \tag{13a}$$

$$= {}_j \left(\frac{\mathcal{W}_j \quad a_j}{a_j \quad {}_i \ a_i} \right) = {}_j \left(\frac{a_j}{{}_i \ a_i} \right) \left(\frac{\mathcal{W}_j}{a_j} \right) \tag{13b}$$

$$= {}_j \left(\frac{a_j}{{}_i \ a_i} \right) G_j \tag{13c}$$

When assuming an isotropic material and neglect the angle between the crack and the load, we can propose as a first approximation for the amount of energy released during the opening of crack j :

$$\mathcal{W}_j = \left(\frac{a_j}{{}_i \ a_i} \right) \quad \mathcal{W} \tag{14}$$

This assumption leads to in Equation (13b) :

$${}_j \left(\frac{a_j}{{}_i \ a_i} \right) \left(\frac{\mathcal{W}_j}{a_j} \right) = {}_j \left(\frac{a_j}{{}_i \ a_i} \right) \left(\frac{a_j}{{}_i \ a_i} \right) \left(\frac{\mathcal{W}}{a_j} \right) \tag{15a}$$

$$= \left(\frac{\mathcal{W}}{{}_i \ a_i} \right) \quad {}_j \left(\frac{a_j}{{}_i \ a_i} \right) = \left(\frac{\mathcal{W}}{{}_i \ a_i} \right) \left(\frac{{}_j \ a_j}{\underline{\ }_i \ \underline{a_i}} \right)_1 \tag{15b}$$

$$= \frac{\mathcal{W}}{a} \tag{15c}$$

Equation (14) is verified and in the case of multiple cracks growing within the same step, the above assumption is equivalent to consider that the same energy is required to open any crack j :

$$G_j = \left[\frac{a_j}{{}_i \ a_i} \quad \mathcal{W} \right] \frac{1}{a_j} \tag{16}$$

Additionally, to evaluate the microstructural effect, the stress-intensity factors are also known to depend on the geometrical configuration of the sample as follows [18, 19] :

$$K = C(a) \ {}_{app} \ \sqrt{a} \tag{17}$$

where $C(a)$ is a dimensionless parameter dependent on sample geometry and loading mode, ${}_{app}$ the applied stress and a the real crack size. ${}_{app}$ is evaluated for the three point bending as follows [20, 21] :

$${}_{app} = \frac{3PH}{2tW^2} \tag{18}$$

where P is the load applied on the sample and S the support pan of the three point bending test device. t and W are the thickness and the width of the sample respectively.

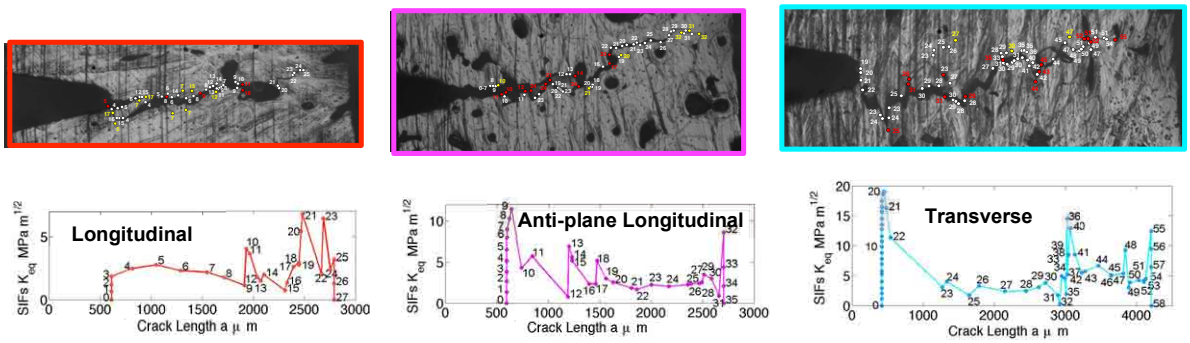

Fig. 6 – Stress intensity factors calculated by total energy variation in the three bone characteristic directions : longitudinal, anti-plane longitudinal, transverse.

4 Conclusions

The analysis of the stress field at the micro scale reveals regions of diffuse damage partially reversible near the cracks [14, 23]. The stress intensity factors calculated by energy variation of the macro response display average values in agreement with the literature [24]. SIFs calculations using the energy variation reveal the toughening effect of the tissue heterogeneity and the Haversian porosity in reducing the SIFs values [25, 23], which is not detected by standard ASTM methods. The Haversian bone microstructure provides positive local toughening to limit crack growth.

Références

[1] J. L. Katz. *Hierarchical modeling of compact Haversian bone as a fiber reinforced material*, Advanced in Bioengineering - ASME, R. E. Mates and C. R. Smith, p.17-18, 1976.

[2] J. Y. Rho, L. Kuhn-Spearing, P. Zioupos, *Mechanical properties and the hierarchical structure of bone*, Medical Engineering and Physics, 20 :92-102, 1998.

[3] K. J. Koester, J. W. Ager III, R. O. Ritchie. *The true toughness of human cortical bone measured with realistically short cracks*, Nature Materials, 7 :672-677, 2008.

[4] P. Fratzl. *When the cracks begin to show*, Nature Materials, 7 :610-612, 2008.

[5] M. R. Forwood, D. Vashishth. *Translational aspects of bone qualityÑvertebral fractures, cortical shell, microdamage and glycation : a tribute to Pierre D. Delmas*, Osteoporosis Int., 20(Suppl 3) :S247-S253, 2009.

[6] B. Philipson. *Composition of cement line in bone*, The Journal of Histochemistry and Cytochemistry, 13(4) :270–281, 1965.

[7] A. K. Egerer, S. Saha, P. J. McMillan, J. Rivera. *Morphology of the cement line in human bone and its relationship to bone strength*, Biomedical Engineering Conference, Proceedings of the 1996 Fifteenth Southern, p.7-10, 1996.

[8] J. D. Currey. *The many adaptations of bone*, Journal of Biomechanics, 36 :1485-1495, 2003.

[9] S. C. Cowin. *Bone mechanics*, CRC Press, Boca Raton, Fl., 1989.

[10] B. Ji, H. Gao. *Mechanical properties of nanostructure of biological materials*, Journal of Mechanics and Physics of Solids, 52 :1963-1990, 2004.

[11] D. B. Burr, R. B. Martin, M. B. Schaffler, E. L. Radin. *Bone remodeling in response to in vivo fatigue microdamage*, Journal of Biomechanics, 18(3) :189-200, 1985.

[12] D. B. Burr, M. B. Shaffler, R. G. Frederickson. *Composition of the cement line and its possible mechanical role as a local interface in human compact bone*, Journal of Biomechanics, 21(11) :939-945, 1988.

[13] P. Zioupos, J. D. Currey, A. J. Sedman. *An examination of the micromechanics of failure of bone and antler by acoustic emission tests and Laser Scanning Confocal microscopy*, Medical Engineering and Physics, 16 :204-213, 1994.

[14] X. Sun, E. McLamore, V. Kishore, K. Fites, M. Slipchenko, D. M. Porterfield, O. Akkus. *Mechanical Stretch Induced Calcium Efflux from Bone Matrix Stimulates Osteoblasts*, Bone, 50, 2012.

[15] M. Bornert, F. Brémand, P. Doumalin. *Assessment of digital image correlation measurement errors : Methodology and results*, Experimental Mechanics, 49(3) :353-370, 2009.

[16] , E. Budyn, J. Jonvaux, T. Hoc. *Digital Image Correlation of Bone Sequential Microscopic Observations*, International Journal for Numerical Methods in Biomedical Engineering, 28(8) :815-837, 2012.

[17] B. Wan, M.A. Sutton, M.F. Petrou, K.A. Harries and N. Li. *Investigation of Bond between Fiber Reinforced Polymer and Concrete Undergoing Global Mixed Mode I/II Loading*, ASCE Journal of Engineering Mechanics, 130, 2004.

[18] J. Lemaitre and J. L. Chaboche. *Mécanique des Matériaux Solides, Seconde Édition*, Dunot, Chapitre 8 : Fissuration, 2004.

[19] J. B. Leblond. *Mécanique de la Rupture Fragile et Ductile*, Hermes Science Publication, 2003.

[20] T. L. Anderson. *Fracture Mechanics : Fundamentals and Applications, Third Edition*, CRCPress, 2004.

[21] H. Tada, P. C. Paris, G. R. Irwin. *The Stress Analysis of Cracks Handbook, Third Edition*, ASM International, 2000.

[22] ASTM E399 - 09e1. *Standard Test Method for Linear-Elastic Plane-Strain Fracture Toughness KIc of Metallic Materials*, ASTM International, 2009.

[23] J. Jonvaux, T. Hoc, E. Budyn. *Analysis of micro fracture in human Haversian cortical bone under compression*, International Journal in Numerical Methods in Biomedical Engineering, 28(9) :974-998, 2012.

[24] R.K. Nalla, J.S. Stölken, J.H. Kinney and R.O. Ritchie. *Fracture in human cortical bone : local fracture criteria and toughening mechanisms*, Journal of Biomechanics, 38, 2005.

[25] E. Budyn and T. Hoc. *Analysis of Micro Fracture in Human Haversian Cortical Bone under transverse tension using Extended Physical Imaging*, International Journal for Numerical Method in Engineering, 2010.